01 Jul 2022

# First-Principles Study of the Thermal Properties of Zr2C and Zr2CO

Yue Zhou

William Fahrenholtz
*Missouri University of Science and Technology*, billf@mst.edu

Joseph T. Graham
*Missouri University of Science and Technology*, grahamjose@mst.edu

Gregory E. Hilmas
*Missouri University of Science and Technology*, ghilmas@mst.edu



## Recommended Citation

Y. Zhou et al., "First-Principles Study of the Thermal Properties of Zr2C and Zr2CO," *Journal of the American Ceramic Society*, vol. 105, no. 7, pp. 4921 - 4929, Wiley, Jul 2022.
The definitive version is available at https://doi.org/10.1111/jace.18461

Received: 10 January 2022 | Revised: 6 March 2022 | Accepted: 9 March 2022

DOI: 10.1111/jace.18461

Journal of the American Ceramic Society

RESEARCH ARTICLE

# First-principles study of the thermal properties of $Zr_2C$ and $Zr_2CO$

Yue Zhou[1] | William G. Fahrenholtz[1] | Joseph Graham[1,2] | Gregory E. Hilmas[1]

[1]Department of Materials Science and Engineering, Missouri University of Science and Technology, Rolla, Missouri, USA

[2]Department of Nuclear Engineering and Radiation Science, Missouri University of Science and Technology, Rolla, Missouri, USA

**Correspondence**
Yue Zhou, Department of Materials Science and Engineering, Missouri University of Science and Technology, Rolla, MO 65409, USA.
Email: yznwb@mst.edu

**Funding information**
Ceramics Program in the Division of Materials Research, U.S. National Science Foundation, Grant/Award Number: DMR 1742086

**Abstract**

First-principles calculations of lattice thermal conductivities and thermodynamic properties of $Zr_2C$ and $Zr_2CO$ were performed using the quasi-harmonic approximation. Oxygen in the lattice gives $Zr_2CO$ higher bonding strength than $Zr_2C$. Thus, the mechanical properties of $Zr_2C$ are enhanced when the vacancies in its crystal structure are filled with oxygen. Among the critical parameters that determine the lattice thermal conductivity, $Zr_2C$ has significantly higher Grüneisen parameters, thus $Zr_2C$ has lower lattice thermal conductivity than $Zr_2CO$. In addition, $Zr_2CO$ has a higher heat capacity and thermal expansion coefficient than $Zr_2C$ at most temperatures. These results indicate that the addition of oxygen has increased the stiffness and thermal conductivity of zirconium carbide that contains a large fraction of carbon vacancies due to the filling of vacancies in the $Zr_2C$ lattice and the formation of Zr–O bonds.

**KEYWORDS**
first-principles theory, thermal conductivity, zirconium/zirconium compounds

## 1 | INTRODUCTION

The reliability of tri-structural isotropic (TRISO) fuel particles is crucial for the performance of future very high-temperature reactors (VHTR) for nuclear power generation.[1] Currently, SiC is the material of choice in TRISO fuel particles. However, swelling of SiC under irradiation is a limitation for its application. ZrC is a candidate to replace SiC in TRISO fuel particles due to its high melting point, high thermal conductivity at very high temperatures, and low neutron absorption cross-sections.[2] It has come to light that ZrC, especially $ZrC_x$ containing significant fractions of carbon vacancies, is chemically and mechanically stable under irradiation and when exposed to fission products.[3–4] In addition, using ZrC in TRISO particles could increase the gas exit temperature of VHTRs, and increase the thermal efficiency as a result.[5] The thermal stability of $ZrC_x$ can also enhance the accident-tolerance of nuclear fuels.[6] Along with nuclear applications, ZrC-W cermets have shown promise as rocket motor components.[7,8] Understanding of thermal, mechanical, and thermodynamic properties of $ZrC_x$ is important for all these applications.

The Zr–C phase diagram produced from experimental data indicates that the carbon stoichiometry of rock salt structured $ZrC_x$ ranges from $x = 0.63$ to 0.98 at 1800°C.[9] First-principles simulations of $ZrC_x$ using mixing enthalpy calculations has predicted that the carbon contents could be as low as $x = 0.5$, wherein an ordered $Zr_2C$ phase could form.[10] In addition, oxygen can dissolve into carbon vacancies in the $ZrC_x$ lattice to form single-phase zirconium oxycarbide.[11] By dissolving oxygen into $ZrC_x$, carbon contents as low as $x = 0.45$ have been predicted to retain the stable rock salt structure with the composition of $ZrC_{0.45}O_{0.55}$.[12] However, these two ordered compounds are not readily synthesized and, as a result, experimental determination of their properties is difficult. The presence of ordered $Zr_2C$ and $Zr_2CO$ phases may influence

  

the properties of $ZrC_x$, but few experimental studies have focused on the properties of these ordered phases and how their presence impact the performance of $ZrC_x$ ceramics. Hence, theoretical predictions of the properties of these two ordered phases are needed.

First-principles calculations have been widely used to predict materials properties. High-throughput materials screening methods are able to identify candidate compositions with desirable properties without time-consuming trial-and-error experimental studies.[13–16] Such methods are especially valuable for investigating the properties of ultra-high-temperature ceramics due to the difficulties in testing materials under extreme conditions.[17] For example, atomistic simulations were used to predict the thermal conductivities of $ZrC_x$ ceramics with carbon stoichiometries ranging from $x = 0.9$ to 1.[18] The thermal conductivities were predicted to increase with increasing temperature as had been observed in experimental studies. Furthermore, the contribution of phonon transport to the total thermal conductivity was negligible at elevated temperatures where the total thermal conductivity was dominated by the electron contribution. The thermal conductivities of $ZrC_x$ ceramics were also investigated for compositions with ordered carbon vacancies.[19] The electron contribution to total thermal conductivity was calculated using the Wiedemann–Franz law while the Debye–Slack model was used to predict the phonon contribution. In general, the thermal conductivity of $ZrC_x$ decreases as the concentration of carbon vacancies increases. Also, the thermal conductivity increases with increasing temperature. The thermal conductivity of ZrC over a wide temperature range was predicted using a single-mode relaxation time approximation to calculate the phonon thermal conductivity, and a semi-classical method was employed to calculate the electron thermal conductivity.[20] The total thermal conductivity was predicted to be affected by grain size, that is, larger grain size favored higher thermal conductivity.

Although the thermal conductivities of $ZrC_x$ were investigated previously, a deeper understanding of the mechanical, thermal, and thermodynamic properties of $Zr_2C$ and $Zr_2CO$ is still needed. Since single-phase $Zr_2C$ and $Zr_2CO$ ceramics have not been experimentally prepared to date. Hence, experimental determination of their properties is difficult, which makes theoretical prediction of their mechanical, thermal, and thermodynamic properties necessary. The purpose of the present paper is to determine the mechanical, thermal, and thermodynamic properties of $Zr_2C$ and $Zr_2CO$ using first-principles calculations and provide basic mechanical, thermal, and thermodynamical data for both compositional control and property tuning of $ZrC_x$.

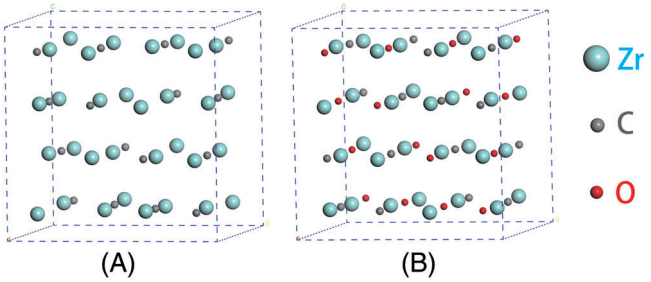


**FIGURE 1** Crystal structures of (A) $Zr_2C$ and (B) $Zr_2CO$

## 2 | CALCULATION METHODS

### 2.1 | First-principles calculations and lattice thermal conductivity

The space group for both $Zr_2C$ and $Zr_2CO$ is $Fd\bar{3}m$. The crystal structures of $Zr_2C$ and $Zr_2CO$, which are shown in Figure 1, were built based on Rietveld refinement of X-ray diffraction patterns.[21] First-principles calculations were employed to optimize the crystal structures and to calculate the second-order elastic constants. Phonon calculations were conducted with the finite displacement method. Once phonon frequencies over the first Brillouin zone are known, the energy of the phonon system ($E$) can be obtained from the canonical distribution in statistical mechanics using the harmonic approximation. Lattice thermal conductivities were predicted using the Debye–Callaway model as reported in our previous papers.[22,23]

### 2.2 | Helmholtz free energy, heat capacity, and coefficient of thermal expansion

Thermodynamic calculations were performed using the quasi-harmonic approximation. Helmholtz free energies $F(V, T)$ were calculated at zero pressure using Equation (1):[24]

$$F(V,T) = E_{\text{tot}} + E_{\text{zp}} + kT \int F(\omega) \ln\left[1 - \exp\left(-\frac{\hbar\omega}{kT}\right)\right] d\omega \quad (1)$$

where $E_{\text{tot}}$ is the total energy at 0 K, $E_{\text{zp}}$ is the zero point vibrational energy, $k$ is the Boltzmann constant, $F(\omega)$ is the phonon density of states, $\hbar$ is the reduced Planck's constant, and $T$ is temperature. The values of $E_{\text{tot}}$ and $E_{\text{zp}}$ were determined using first-principles calculations.

Heat capacity at constant pressure was calculated using Equation (2):

$$C_{\text{P}} = C_{\text{v}} + \alpha_{\text{v}}^2 BVT \quad (2)$$

where $B$ is the bulk modulus, $V$ is the equilibrium volume of the crystal structures, and $\alpha_v$ is the volume thermal expansion coefficient determined from the Helmholtz free energy ( $\alpha_v = \partial \ln V / \partial T$ ) with $C_v$ calculated using Equation (3):

$$C_v = C_v^{ph} + C_v^{el} \tag{3}$$

where $C_v^{ph}$ is the phonon heat capacity given by:

$$C_v^{ph} = k_B \sum_{j,q} \frac{(\hbar\omega_{jq})^2 e^{\hbar\omega_{jq}/k_B T}}{(k_B T)^2 \left(e^{\hbar\omega_{jq}/k_B T} - 1\right)^2} \tag{4}$$

The phonons are summed over branch index $j$ and wave vector $\boldsymbol{q}$. $C_v^{el}$ is the electron heat capacity at different temperatures given by:

$$C_v^{el} = \gamma T \tag{5}$$

where

$$\gamma = \frac{1}{3}\pi^2 N(E_F) k_B^2 \tag{6}$$

and $N(E_F)$ is the electron density of states at the Fermi level.

The phonon properties change with the volume since the interatomic potential is an asymmetric function of interatomic spacing (and therefore volume). The volume dependence of the phonon properties was obtained by calculating the phonon dispersions for $Zr_2C$ and $Zr_2CO$ at 13 different volumes to obtain the thermodynamic parameters. The lattice constants of the $Zr_2C$ primitive cells ranged from 6.5778 to 7.0395 Å while the lattice constants for $Zr_2CO$ primitive cells ranged from 6.5795 to 6.6242 Å. The Vinet equation of state[25] was employed to fit the free energies and equilibrium volumes at different temperatures. Bulk modulus ($B$) and equilibrium volumes ($V$) were obtained by fitting the outputs.

## 3 | RESULTS AND DISCUSSION

### 3.1 | Lattice parameters and mechanical properties

The calculated lattice parameters of $Zr_2C$ and $Zr_2CO$ are listed in Table 1. Compared to the lattice parameter of $Zr_2C$ (9.441 Å), the lattice parameter of $Zr_2CO$ is lower (9.336 Å) due to the presence of oxygen atoms in the $Zr_2CO$ lattice instead of the vacancies in $Zr_2C$. In the crystal structure of $Zr_2C$, the average distance between neighboring Zr atoms along the crystallographic axes is 4.714 Å, which is larger than that of $Zr_2CO$ (4.671 Å). The reduction has been explained by the formation of Zr–O bonds, which increases the average bond strength in the lattice and, therefore, decreases the distance between neighboring Zr atoms.[26,27] The reduction in lattice parameter, increase in bond strength, and increase in the number of bonds when oxygen is inserted into vacancies in the $Zr_2C$ lattice should enhance the elastic moduli of $Zr_2CO$ compared to $Zr_2C$.

**TABLE 1** Lattice parameters ($a$) (Å), second-order elastic constants ($c_{11}$, $c_{44}$, $c_{12}$) (GPa), shear modulus $G$ (GPa), bulk modulus $B$ (GPa), elastic modulus $E$ (GPa), Poisson's ratio $\nu$, and microhardness $H_V$ (GPa) of $Zr_2C$, and $Zr_2CO$ from the present study and, for comparison, ZrC from a previous study.[22] Values in parentheses are first principle predictions for $Zr_2C$ from a previous study[28]

| Composition | ZrC[22] | $Zr_2C$ | $Zr_2CO$ |
|---|---|---|---|
| Lattice constant $a$ (Å) | 4.706 | 9.411, (*9.369*)[28] | 9.336 |
| $c_{11}$ | 452 | 203 | 373 |
| $c_{44}$ | 155 | 99 | 98 |
| $c_{12}$ | 107 | 91 | 111 |
| $G$ | 162 | 82, (*71*)[28] | 111 |
| $B$ | 222 | 128, (*137*)[28] | 198 |
| $E$ | 391 | 203 | 281 |
| $\nu$ | 0.21 | 0.24 | 0.26 |
| $H_V$ | 24.2 | 12.6, (*8.4*),[28] (*10.8*)[28] | 13.0 |

The calculated elastic constants and Poisson's ratio for both compounds are listed in Table 1 with values from other reports[22,28] included for comparison. The elastic constants are a direct reflection of bond strength. Two of the second-order elastic constants, $c_{11}$ and $c_{12}$, increase as oxygen atoms are inserted into $Zr_2C$ to form $Zr_2CO$ ($c_{11}$ = 203 GPa for $Zr_2C$ and 373 GPa for $Zr_2CO$, $c_{12}$ = 91 GPa for $Zr_2C$ and 111 GPa for $Zr_2CO$). Even though $c_{44}$ of $Zr_2CO$ (98 GPa) is slightly lower than that of $Zr_2C$ (99 GPa), the shear modulus, bulk modulus, elastic modulus, and microhardness of $Zr_2CO$ all increase as oxygen is added to the lattice. For example, $E$ increases from 203 GPa for $Zr_2C$ to 281 GPa for $Zr_2CO$, while hardness increases from 12.6 to 13.0 GPa. Compared to pure ZrC with all of the carbon sites occupied by carbon atoms, only one second-order elastic constant, $c_{12}$, of $Zr_2CO$ is larger than that of ZrC ($c_{12}$ = 107 GPa for ZrC and 111 GPa for $Zr_2CO$). The other two second-order elastic constants and all the other mechanical properties of bulk polycrystalline $Zr_2CO$ are lower than ZrC. A similar decrease in hardness and elastic constants has been observed experimentally when oxygen replaces carbon in the ZrC lattice.[26]

### 3.2 | Phonon dispersion and density of states

Phonon dispersion curves along high-symmetry directions in the Brillouin zone and the phonon density of states of

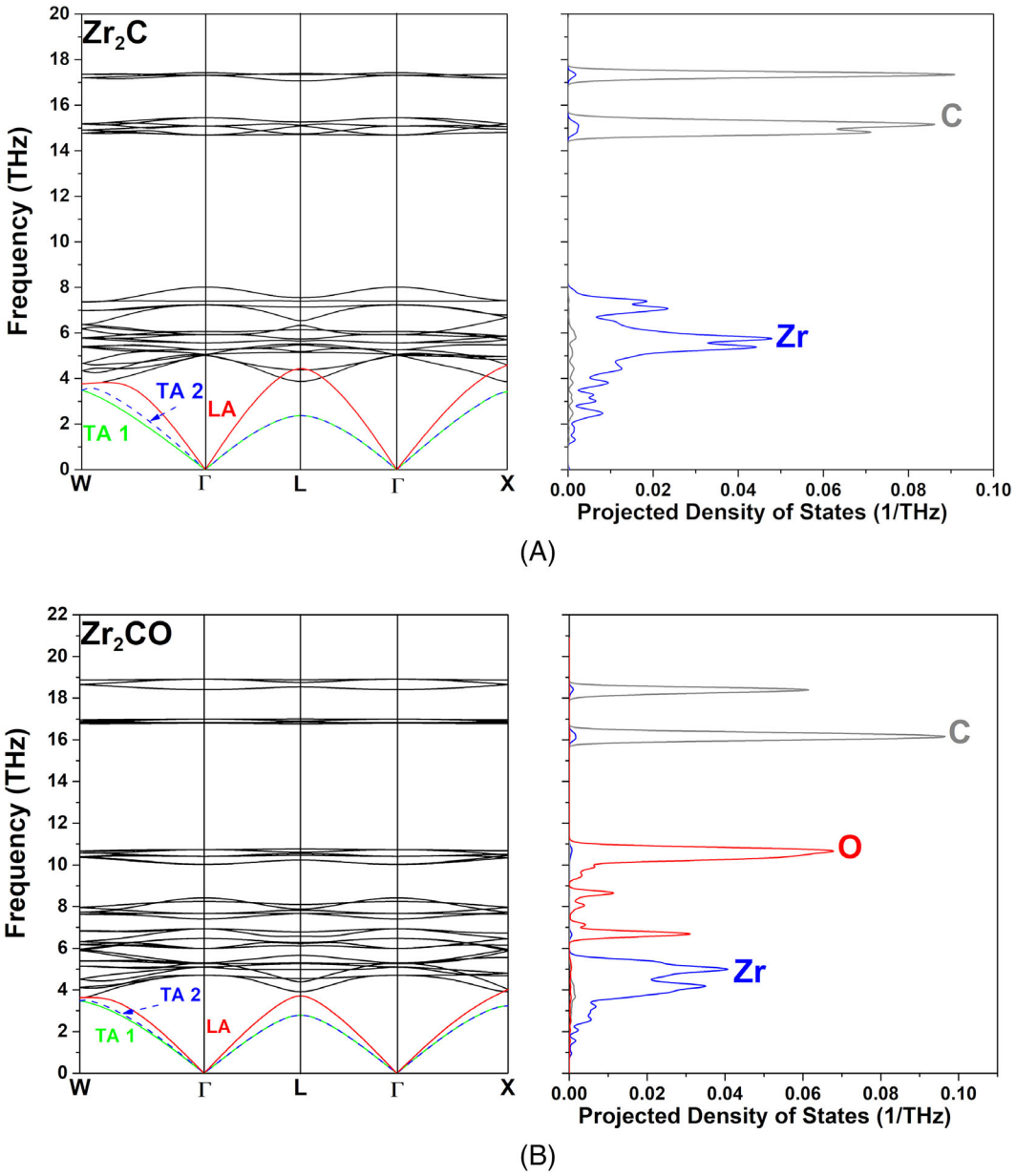


**FIGURE 2** Phonon dispersions and density of states for (A) $Zr_2C$ and (B) $Zr_2CO$

$Zr_2C$ and $Zr_2CO$ are shown in Figure 2. The colored lines in the dispersion curves are the acoustic phonon branches, which include two transverse (TA1, TA2) and one longitudinal (LA) branches. The black lines are the optical phonon branches. From the phonon dispersion curves, no obvious gap is present between the acoustic phonon and low-lying frequency optical phonon branches. The slopes of the high-frequency optical phonons are relatively flat compared to the acoustic phonons, which indicates that the contributions of high-frequency optical phonons to the lattice thermal conductivities can be ignored. The lack of an obvious gap between the acoustic and optical phonon branches is an indication of interactions between them. The low-frequency optical phonon branches overlap with the longitudinal acoustic phonon branch for $Zr_2C$ as shown in Figure 2A, which indicates that acoustic phonons are scattered by moderate-frequency optical phonons. The projected density of states of $Zr_2C$ illustrates that low-frequency phonon branches are mostly related to Zr atoms, while high-frequency phonon branches are primarily associated with C atoms. The higher frequency of phonon branches of C atoms indicates that Zr–C bonds are stronger than Zr–Zr bonds. Phonon dispersion and the projected density of states of $Zr_2CO$ are shown in Figure 2B. Low-frequency optical phonon branches scatter the acoustic phonon branches in $Zr_2CO$ as well since they overlap. Phonon frequencies of O atoms are between Zr and C atoms as shown in the projected density of states in the

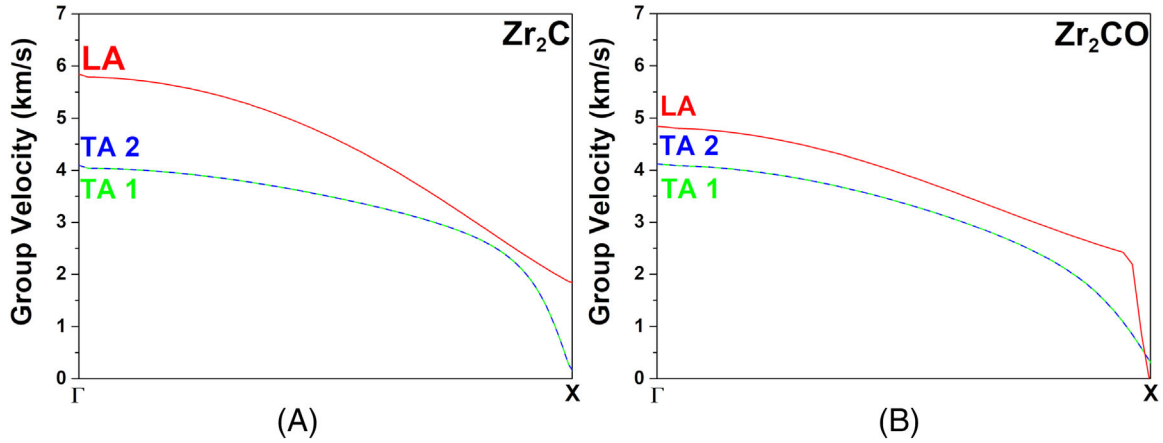


**FIGURE 3** Group velocities for (A) $Zr_2C$ and (B) $Zr_2CO$

**TABLE 2** The group velocities, Debye temperatures, and Grüneisen parameters for ZrC[22], $Zr_2C$, $Zr_2CO$ and compared with a thermally insulating material $Gd_2Zr_2O_7$[33]

| Unit / Composition | $\upsilon_{TA1}$ (km/s) | $\upsilon_{TA2}$ (km/s) | $\upsilon_{LA}$ (km/s) | $\theta_{TA1}$ (K) | $\theta_{TA2}$ (K) | $\theta_{LA}$ (K) | $\gamma_{TA1}$ N/A | $\gamma_{TA2}$ N/A | $\gamma_{LA}$ N/A |
|---|---|---|---|---|---|---|---|---|---|
| ZrC[22] | 4.2 | 4.2 | 8.0 | 340.5 | 340.5 | 467.0 | 1.8 | 1.5 | 1.7 |
| $Zr_2C$ | 4.1 | 4.1 | 5.8 | 167.5 | 172.7 | 220.1 | 10.0 | 9.1 | 4.3 |
| $Zr_2CO$ | 4.1 | 4.1 | 4.8 | 167.1 | 168.2 | 192.9 | 2.1 | 1.5 | 2.8 |
| $Gd_2Zr_2O_7$[33] | 3.06 | 3.06 | 5.63 | 137 | 137 | 252 | 7.19 | 11.57 | 2.75 |

figure, which indicates that Zr–O bonds are weaker than Zr–C bonds.

Lattice thermal conductivity in any specific direction at low temperature is proportional to the square of group velocity, that is, $\kappa_s(\omega) = C_s(\omega)V_g(\omega)^2\tau(\omega)$.[29] Thus, calculating the group velocities of $Zr_2C$ and $Zr_2CO$ (Figure 3) provides insight into thermal conducting behavior. The group velocities along the [100] direction of $Zr_2C$ are $\upsilon_{TA1} = \upsilon_{TA2} = 4.1$ km s$^{-1}$, $\upsilon_{LA} = 5.8$ km s$^{-1}$; while those of $Zr_2CO$ are $\upsilon_{TA1} = \upsilon_{TA2} = 4.1$ km s$^{-1}$, $\upsilon_{LA} = 4.8$ km s$^{-1}$ (Table 2). The difference between group velocities of $Zr_2CO$ and $Zr_2C$ is small, indicating that any differences in their lattice thermal conductivities will be indicated by the Grüneisen parameters.

The Debye temperatures of the acoustic transverse and longitudinal phonon branches were calculated using the relationship $\theta_i = \hbar\omega_{max}/k_B$, where $\hbar$ is the reduced Planck constant, $\omega_{max}$ represents the maximum frequency of the phonon branches at the boundary of the Brillouin zone, and $k_B$ is the Boltzmann constant.[30] The Debye temperature is a factor that affects the partial thermal conductivity of each branch. For $Zr_2C$, the Debye temperature does not change significantly as oxygen atoms are introduced into the crystal structure. For example, $\theta_{TA1}$ slightly decreases from 167.5 K for $Zr_2C$ to 167.1 K for $Zr_2CO$ while $\theta_{TA2}$ decreases from 172.7 to 168.2 K and $\theta_{LA}$ decreases from 220.1 to 192.9 K. Based on this analysis, those parameters are not the factors that have a significant effect on differences in the lattice thermal conductivity for $Zr_2CO$ compared to $Zr_2C$.

Grüneisen parameters are affected by the relationship between the change in phonon frequency with the change in volume of the crystal structure[31] in addition to being a factor that can be used to calculate the relaxation times of normal and Umklapp scattering processes. The Grüneisen parameters of $Zr_2C$, especially for the transverse acoustic phonon branches ($\gamma_{TA1}$ and $\gamma_{TA2}$), are significantly higher than those of $Zr_2CO$. The parameter values of $Zr_2C$ ($\gamma_{TA1} = 10.0$, $\gamma_{TA2} = 9.1$, $\gamma_{LA} = 4.3$) are higher than those for materials that are typically considered to be good thermal conductors.[32] Thus, a material with a low lattice thermal conductivity, $Gd_2Zr_2O_7$,[33] was used to compare with the data in the present study ( $\gamma_{TA1} = 7.19$, $\gamma_{TA2} = 11.57$, $\gamma_{LA} = 2.75$) based on the similarly high values of Grüneisen parameters. Both $Gd_2Zr_2O_7$ and $Zr_2C$ have large concentrations of vacancies neighboring Zr atoms, giving rise to highly asymmetric and anharmonic interatomic potentials. At high temperatures, the anharmonic terms in the potentials enhance Umklapp scattering, which, in turn, reduces the lattice thermal

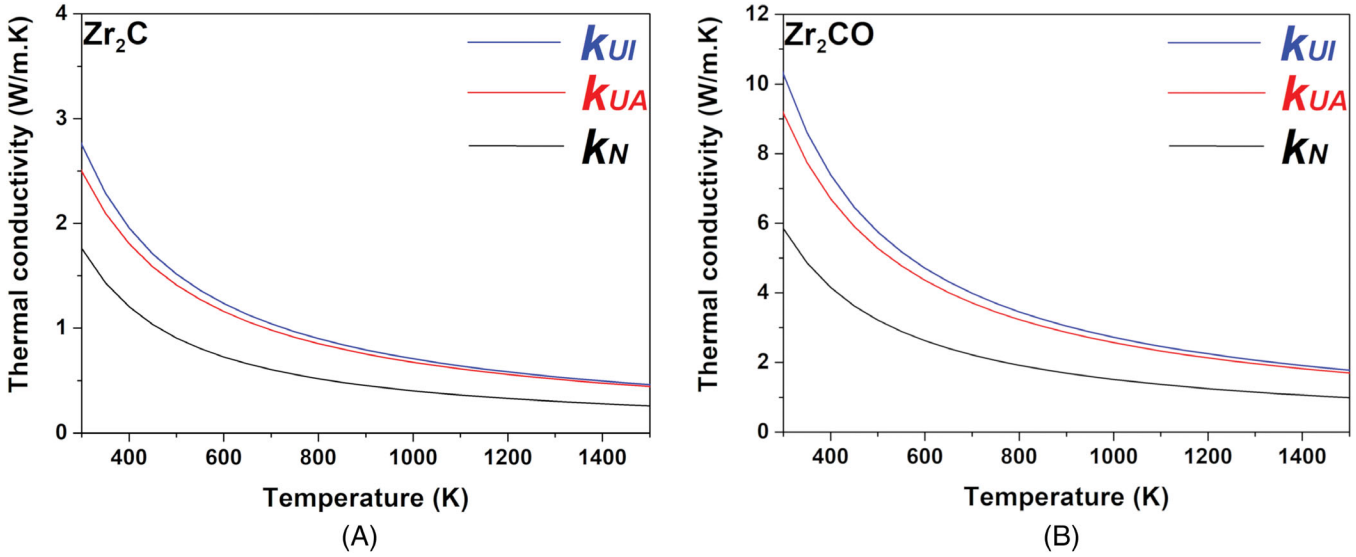


**FIGURE 4** Lattice thermal conductivities of (A) $Zr_2C$ and (B) $Zr_2CO$ ($K_{UI}$: isotope effect; $K_{UA}$: isotope and grain boundary effects; $K_N$: isotope, grain boundary, Umklapp, and normal processes effects)

conductivity. The Grüneisen parameters of $Zr_2CO$ are lower than $Zr_2C$ due to the more symmetric interatomic potential of Zr in a O–Zr–C chain compared to Zr in $Zr_2C$ that has a chain of vacancy–Zr–C. However, the electronic contribution can dominate the thermal conductivity at elevated temperatures. Thus, $Zr_2C$ may not necessarily have a lower total thermal conductivity than $Zr_2CO$, but its lattice thermal conductivity is lower. The effects of electron–carbon vacancy scattering, electron–oxygen scattering, and the electron–phonon interaction would need to be analyzed to provide additional insight into the electron contribution to the total thermal conductivity.

Compared to ZrC, the intrinsic lattice thermal conductivity of $ZrC_x$ decreases as the number of carbon vacancies in the lattice increases. $Zr_2CO$ also has a lower lattice thermal conductivity than ZrC.[22] Therefore, replacing carbon atoms with oxygen atoms decreases the thermal conductivity of $ZrC_x$. This is expected as O atoms represent larger mass defects than carbon isotopes do. Comparing the key parameters for lattice thermal conductivity of ZrC and $Zr_2CO$ (Table 2), the Debye temperature decreases significantly when oxygen replaces carbon atoms in the lattice because replacing carbon with oxygen decreases the frequency of the lattice vibrations.[34]

## 3.3 | Lattice thermal conductivity

Figure 4 shows the temperature-dependent lattice thermal conductivities of $Zr_2C$ and $Zr_2CO$ that were calculated using a combination of first-principles calculations and the Debye–Callaway model. The effects of Zr isotopes, grain boundaries, and Umklapp and normal processes were considered in these calculations as detailed in our previous studies.[22,23] The lattice thermal conductivities for both ordered compounds at elevated temperatures are significantly lower than those at room temperature due to phonon scattering.[25] The lattice thermal conductivity of $Zr_2C$ increases with the insertion of O atoms into the crystal structure to form $Zr_2CO$. The room temperature lattice thermal conductivity ($\kappa_N$) of $Zr_2C$ is 1.76 W $m^{-1}$ $K^{-1}$, which increases to 5.85 W $m^{-1}$ $K^{-1}$ for $Zr_2CO$. The increased lattice thermal conductivity agrees with the expectations based on the group velocities and Grüneisen parameters discussed above.

## 3.4 | Thermodynamic properties

Heat capacity ($C_P$) is a fundamental thermodynamic property and one of the factors that affects thermal conductivity ($\kappa$) of materials based on the relationship $k = D\rho C_P$, where $D$ is thermal diffusivity and $\rho$ is the density. The heat capacities of $Zr_2C$ and $Zr_2CO$ were not calculated in previous studies. For the present study, calculation of the heat capacity of ZrC is used to validate the methods used to predict heat capacities for $Zr_2C$ and ZrCO. The black line in Figure 5A is the heat capacity of ZrC calculated by the current method, which fits well with the previous results calculated using quasi-harmonic Debye, Debye–Slater, and Debye–Grüneisen models.[35,36] Heat capacities of $Zr_2C$ and $Zr_2CO$ at constant pressure are also shown in Figure 5B. When the contributions from phonons and electrons are considered, the heat capacities for both $Zr_2C$ and $Zr_2CO$ increase as temperature increases. $Zr_2CO$ has a higher heat capacity than $Zr_2C$ over the entire temperature

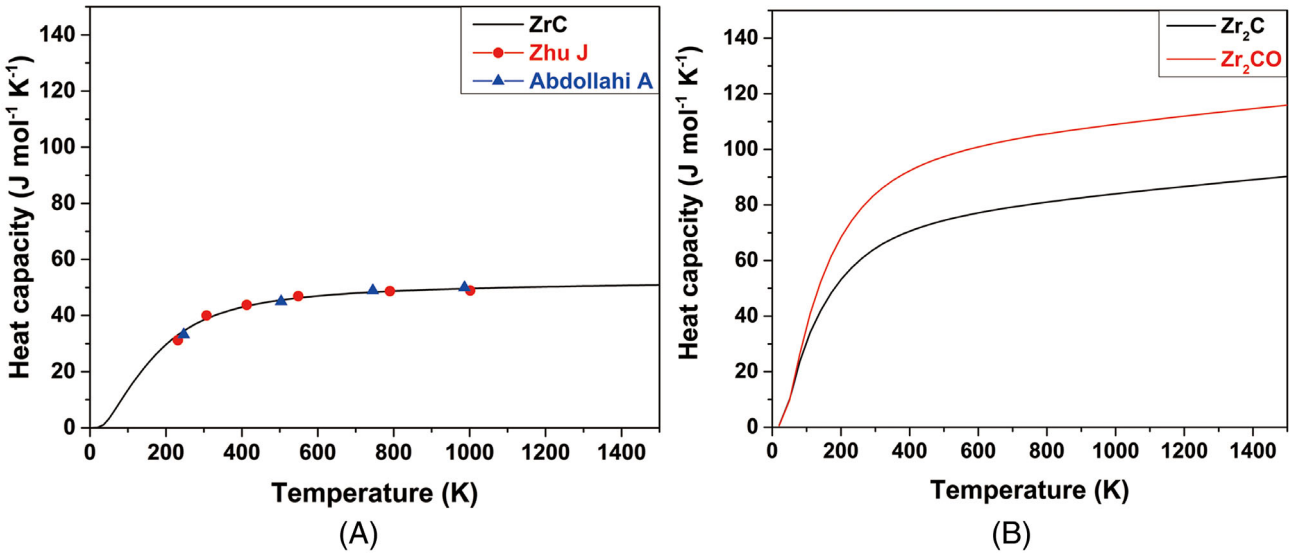


**FIGURE 5** The heat capacities of (A) ZrC and (B) $Zr_2C$ and $Zr_2CO$

range. This is expected as $Zr_2CO$ has more atoms and, therefore, on a molar basis will have 33% more degrees of freedom. For the parameters that affect heat capacity at constant pressure ($C_P$), $Zr_2CO$ has higher electron ($C_v^{el}$) and phonon heat capacities ($C_v^{ph}$) and thus has higher heat capacity at constant volume ($C_v$). That is another indication that $Zr_2CO$ has a higher thermal conductivity than $Zr_2C$.

Thermal expansion coefficients of ZrC, $Zr_2C$, and $Zr_2CO$ as function of temperature are shown in Figure 6. The volume thermal expansion coefficient of ZrC calculated using the methods in the current study is compared with values from simulations using the quasi-harmonic approximation,[36] as well as with experimental values[37] as shown in Figure 6A. Values from the theoretical studies are higher than the experimental values because the simulations do not consider defects, flaws, or impurities. The linear thermal expansion of ZrC ($8.84 \times 10^{-6}$ $K^{-1}$) is lower than $Zr_2C$ ($8.90 \times 10^{-6}$ $K^{-1}$) and $Zr_2CO$ ($10.06 \times 10^{-6}$ $K^{-1}$). The linear thermal expansion coefficient of $Zr_2C$ is lower than $Zr_2CO$ across most of the temperature range. For example, at 292 K, thermal expansion coefficient of $Zr_2C$ is $6.49 \times 10^{-6}$ $K^{-1}$, and $Zr_2CO$ is $7.34 \times 10^{-6}$ $K^{-1}$. The thermal expansion coefficient of $Zr_2C$ increases less as a function of temperature than $Zr_2CO$ and reaches a plateau value above 600 K. However, the thermal expansion value of $Zr_2CO$ does not reach a plateau as temperature increases. Below 200 K, the thermal expansion coefficient increases rapidly as temperature increases, then tend to slow between 200 and 800 K. Above 800 K, the rate of increase in the thermal expansion coefficient rises again. The increasing rate of thermal expansion coefficient at high temperature indicates that $Zr_2CO$ is less thermally stable than ZrC or $Zr_2C$.

## 4 | CONCLUSION

The elastic, thermal, and thermodynamic properties of ordered $Zr_2C$ and $Zr_2CO$ were studied theoretically. The bond strength of $Zr_2C$ increased as oxygen atoms occupied the carbon vacancy sites, which was manifested as a decrease in the lattice parameter as oxygen substituted into carbon vacancy sites. Second-order elastic constants and mechanical properties were calculated to assess the intrinsic lattice thermal conductivity. $Zr_2CO$ possessed higher values of hardness and elastic constants than $Zr_2C$. Phonon dispersions at different volumes were calculated for both compositions. Phonon density of states were analyzed to interpret the bonding strength. Lattice thermal conductivities of $Zr_2C$ and $Zr_2CO$ were calculated using a combination of first-principles calculations and the Debye–Callaway model. Group velocity, Debye temperature, and Grüneisen parameter were also analyzed. $Zr_2CO$ had higher lattice thermal conductivity than $Zr_2C$ due to the lower Grüneisen parameters which is crucial to determine the lattice thermal conductivity. Thermal expansion coefficients and heat capacities were also calculated for both crystal structures. The thermal expansion coefficient of $Zr_2CO$ was larger than $Zr_2C$ when the temperature was higher than 110 K. However, the thermal expansion coefficient of $Zr_2CO$ varied across the entire range of temperatures investigated, indicating its instability at high temperatures. The heat capacity of $Zr_2CO$ was higher than $Zr_2C$,

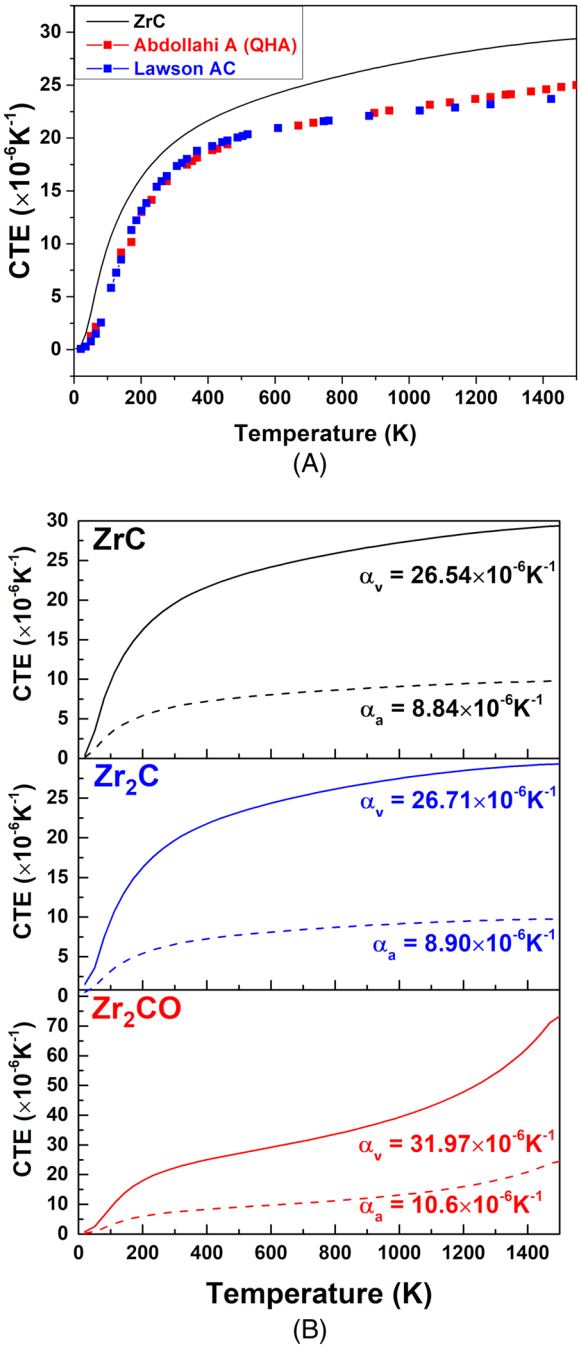


**FIGURE 6** (A) Coefficient of thermal expansion of ZrC compared to quasi-harmonic approximation predictions[36] and experimental values.[37] (B) Volumetric and linear coefficients of themral expansion of Zr, $Zr_2C$, and $Zr_2CO$ at different temperatures

which was one reason that $Zr_2CO$ had a higher lattice thermal conductivity than $Zr_2C$.

## ACKNOWLEDGEMENTS

The authors would like to acknowledge the financial support from the Ceramics Program in the Division of Materials Research, U.S. National Science Foundation (DMR 1742086). The first-principles calculations for the current study were supported by National Supercomputing Center in Shenzhen, China.

## ORCID

*Yue Zhou* https://orcid.org/0000-0001-6901-947X
*William G. Fahrenholtz* https://orcid.org/0000-0002-8497-0092

## REFERENCES

1. Porter IE, Knight TW, Dulude MC, Roberts E, Hobbs J. Design and fabrication of an advanced TRISO fuel with ZrC coating. Nucl Eng Des. 2013;259:180–6.
2. Ueta S, Aihara J, Yasuda A, Ishibashi H, Takayama T, Sawa K. Fabrication of uniform ZrC coating layer for the coated fuel particle of the very high temperature reactor. J Nucl Mater. 2008;376(2):146–51.
3. Reynolds GH, Janvier JC, Kaae JL, Morlevat JP. Irradiation behavior of experimental fuel particles containing chemically vapor deposited zirconium carbide coatings. J Nucl Mater. 1976;62(1):9–16.
4. Wei B, Wang D, Wang Y, Zhang H. Microstructure evolution in ZrCx with different stoichiometries irradiated by four MeV Au ions. Materials 2019;12(22):3768.
5. Wagner P. High-temperature fuel technology for nuclear process heat: ZrC-containing coated particle fuels and high-density graphite fuel matrices. No. LA-6984. New Mexico, USA: Los Alamos Scientific Lab; 1977.
6. Chen L, Lei Y, Li W, Zhang J, Wang J. Thermal stability and performance of optimized ZrCx diffusion barriers in ceramic coating systems for ATF applications. J Am Ceram Soc. 2021;104(10):5424–31.
7. Song GM, Wang YJ, Zhou Y. Elevated temperature ablation resistance and thermophysical properties of tungsten matrix composites reinforced with ZrC particles. J Mater Sci. 2001;36(19):4625–31.
8. Dickerson MB, Wurm PJ, Schorr JR, Hoffman WP, Wapner PG, Sandhage KH. Near net-shape, ultra-high melting, recession-resistant ZrC/W-based rocket nozzle liners via the displacive compensation of porosity (DCP) method. J Mater Sci. 2004;39(19):6005–15.
9. Sara RV. The system zirconium—carbon. J Am Ceram Soc. 1965;48(5):243–7.
10. Zhang Y, Liu B, Wang J. Self-assembly of carbon vacancies in sub-stoichiometric $ZrC_{1-x}$. Sci Rep. 2015;5(1):1–9.
11. Sarkar SK, Miller AD, Mueller JI. Solubility of oxygen in ZrC. J Am Ceram Soc. 1972;55(12):628–30.
12. Henney J, Jones JWS. Ternary phases in the zirconium-carbon-oxygen system. UK Atomic Energy Authority Research Group; 1964.
13. Liu B, Zhao J, Liu Y, Xi J, Li Q, Xiang X, et al. Application of high-throughput first-principles calculations in ceramic innovation. J Mater Sci Technol. 2021;88:143–57.
14. Xiang HM, Feng ZH, Li ZP, Zhou YC. First-principles investigations on elevated temperature elastic and thermodynamic properties of ZrB2 and HfB2. J Am Ceram Soc. 2017;100:3662–72.
15. Xiang HM, Feng ZH, Li ZP, Zhou YC. Temperature-dependence of structural and mechanical properties of TiB2: a first principle investigation. J Appl Phys. 2015;117:2259021–8.

16. Xiang HM, Zhou YC. Phonon engineering in tuning the thermal conductivity of alkaline-earth hexaborides. J Eur Ceram Soc. 2020;40:1352–60.
17. Nath P, Plata JJ, Santana-Andreo J, Blancas EJ, Márquez AM, Sanz JF. High-throughput screening of the thermoelastic properties of ultrahigh-temperature ceramics. ACS Appl Mater Interfaces. 2021;13(25):29843–57.
18. Crocombette JP. Origins of the high temperature increase of the thermal conductivity of transition metal carbides from atomistic simulations. J Phys Condens Matter. 2013;25(50):505501.
19. Zhang Y, Liu B, Wang J, Wang J. Theoretical investigations of the effects of ordered carbon vacancies in $ZrC_{1-x}$ on phase stability and thermo-mechanical properties. Acta Mater. 2016;(111):232–41.
20. Mellan TA, Aziz A, Xia Y, Grau-Crespo R, Duff AI. Electron and phonon interactions and transport in the ultrahigh-temperature ceramic ZrC. Phys Rev B. 2019;99:094310
21. Hu W, Xiang J, Liu S, Zhang Y, Chen C, Wang P, et al. Low-temperature diffusion of oxygen through ordered carbon vacancies in Zr2Cx: the formation of ordered Zr2CxOy. Inorg Chem. 2012;51(9):5164–72.
22. Zhou Y, Fahrenholtz WG, Graham J, Hilmas GE. From thermal conductive to thermal insulating: Effect of carbon vacancy content on lattice thermal conductivity of ZrCx. J Mater Sci Technol. 2021;82:105–113.
23. Zhou Y, Fahrenholtz WG, Graham J, Hilmas GE. Electronic structure and thermal conductivity of zirconium carbide with hafnium additions. J Am Ceram Soc. 2021;104(9):4708–17.
24. Baroni S, Stefano DG, Andrea DC, Giannozzi O. Phonons and related crystal properties from density-functional perturbation theory. Rev Mod Phys. 2001;73(2):515.
25. Ogawa T, Ikawa K. Crushing strengths of SiC-Triso and ZrC-Triso coated fuel particles. J Nucl Mater. 1981;98:18–26.
26. Barnier P, Thévenot F. Synthesis and hot-pressing of single-phase $ZrC_xO_y$ and two-phase $ZrC_xO_y$–$ZrO_2$ materials. Int J High Tech Ceram. 1986;2(4):291–307.
27. Gendre M, Maître A, Trolliard G. Synthesis of zirconium oxycarbide (ZrCxOy) powders: influence of stoichiometry on densification kinetics during spark plasma sintering and on mechanical properties. J Eur Ceram Soc. 2011;31(13):2377–85.
28. Xie CW, Oganov AR, Li D, Debela TT, Liu N, Dong D, et al. Effects of carbon vacancies on the structures, mechanical properties, and chemical bonding of zirconium carbides: a first-principles study. Phys Chem. Chem. Phys. 2016;18(17):12299–306.
29. Toberer ES, Zevalkink A, Snyder GJ. Phonon engineering through crystal chemistry. J Mater Chem. 2011;21(40):15843–52.
30. Zhang Y. First-principles Debye–Callaway approach to lattice thermal conductivity. J Materiomics. 2016;2(3):237–47.
31. Grimvall G. Thermophysical properties of materials. Amsterdam, Netherlands: Elsevier; 1999.
32. Xiang HM, Wang JM, Zhou YC. Theoretical predictions on intrinsic lattice thermal conductivity of ZrB2. J Eur Ceram Soc. 2019;39:2982–8
33. Lan G, Ouyang B, Song J. The role of low-lying optical phonons in lattice thermal conductance of rare-earth pyrochlores: a first-principle study. Acta Mater. 2015;91:304–17.
34. Toberer ES, Zevalkink A, Snyder GJ. Phonon engineering through crystal chemistry. J Mater Chem. 2011;40(21):15843–52.
35. Zhu J, Zhu B, Qu J, Gou Q, Chen F. Thermodynamic properties of cubic ZrC under high pressure from first-principles calculations. Sci China Ser G Phys Mech Astron. 2009;52(7):1039–42.
36. Abdollahi A. First-principle calculations of thermodynamic properties of ZrC and ZrN at high pressures and high temperatures. Phys B. 2013;410:57–62.
37. Lawson AC, Butt DP, Richardson JW, Li J. Thermal expansion and atomic vibrations of zirconium carbide to 1600 K. Philos Mag. 2007;17(87):2507–19.

**How to cite this article:** Zhou Y, Fahrenholtz WG, Graham J, Hilmas GE. First-principles study of the thermal properties of $Zr_2C$ and $Zr_2CO$. J Am Ceram Soc. 2022;105:4921–4929.
https://doi.org/10.1111/jace.18461